6ICEGE 6th International Conference on Earthquake Geotechnical Engineering
1-4 November 2015
Christchurch, New Zealand

Dissipative Behaviour of Reinforced-earth Retaining Structures Under Severe Ground Motion

L. Masini[1], L. Callisto[2], S. Rampello[3]

ABSTRACT

This paper focuses on the seismic performance of geosynthetic-reinforced retaining walls (GRWs) that several evidences have shown to be generally adequate. This can be attributed to the dissipation of energy produced by the internal plastic mechanisms activated during the seismic shaking, and to an overall ductile behaviour related to the large deformation that can be accommodated by the soil-reinforcement system. Using a number of numerical computations, this work compares the behaviour of three idealized structures that were conceived in order to have a similar seismic resistance, that however is activated through different plastic mechanisms. The analyses include numerical pseudo-static computations, carried out iteratively to failure, and time-domain nonlinear dynamic analyses, in which acceleration time-histories were applied to the bottom boundary of the same numerical models used for the pseudo-static analyses. The results of the dynamic analyses were interpreted in the light of the plastic mechanisms obtained with the pseudo-static procedure, confirming that GRWs develop local plastic mechanisms during strong motion resulting in a significant improvement of their seismic performance.

Analysis of Plastic Mechanisms

Several field observations have shown a generally good performance of geosynthetic-reinforced earth retaining structures subjected to severe seismic loading (e.g. Koseki et al., 2009), and this finding is consistent with observations resulting from shaking table experiments on model reinforced-earth structures (Ling et al., 2005). Reasonably, this satisfactory behaviour can be ascribed to the possibility that these structures contribute to energy dissipation through the development of internal plastic mechanisms, and posses an overall ductile behaviour deriving from the large deformation that can be accommodated by the soil-reinforcement system. These plastic mechanisms may mobilize the strength of different portions of the system, including the reinforcing elements, the soil-reinforcement interfaces, the retained soil, and possibly the foundation soil.

This paper examines the behaviour of three different idealized structures retaining the same backfill and resting on the same foundation soil. Specifically, the backfill is 15 m high and has a batter $\beta = 10°$ (Figure 1). Cases (A) and (B) refer to two GRWs with 25 geo-grid layers installed at uniform spacing $s = 0.6$ m. For case (A), reinforcements have a length $B = 11.25$ m ($B/H = 0.75$) and a tensile strength $T_T = 25$ kN/m, while for case (B) they are shorter ($B = 7.9$ m, $B/H = 0.53$) but stronger ($T_T = 35$ kN/m). For case (C), a conventional gravity retaining structure with a base $B = 5.6$ m ($B/H = 0.38$) is considered. Typically, traditional retaining walls such as

[1]Res. Fellow, Dpt. of Struct. and Geotech. Eng., Sapienza Univ. di Roma, Rome, Italy, luca.masini@uniroma1.it
[2]Ass. Prof., Dpt. of Struct. and Geotech. Eng., Sapienza Univ. di Roma, Rome, Italy, luigi.callisto@uniroma1.it
[3]Prof., Dpt. of Struct. and Geotech. Eng., Sapienza Univ. di Roma, Rome, Italy, sebastiano.rampello@uniroma1.it

masonry or lightly reinforced concrete walls, possess a strong internal strength but low dissipative capabilities and exhibit a poor ductile behaviour. In this study it is assumed that, for a conventional gravity wall subjected to a severe ground motion, energy dissipation takes place mostly for the development of plastic mechanisms within the soil, which must be activated before the internal strength of the structure is attained. Therefore, in the analyses wall (C) is modelled as a purely elastic material to reproduce its limited capability to dissipate the earthquake-induced kinematic energy.

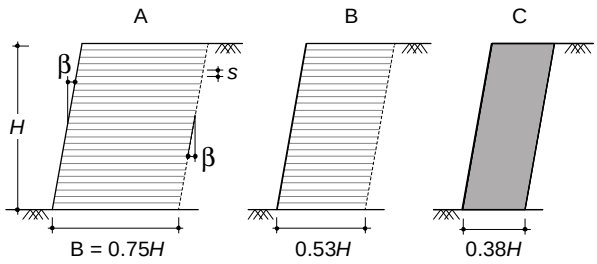

Figure 1. Layouts of the three idealised earth retaining structures

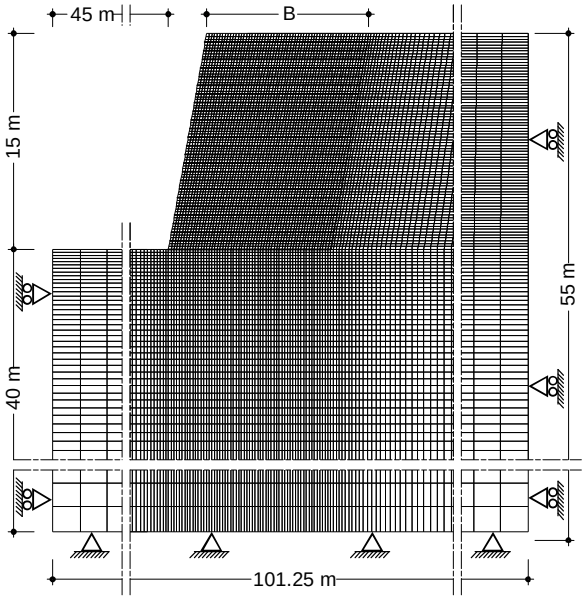

Figure 2. Detail of the finite difference grid adopted for case (A), showing the boundary conditions adopted in the pseudo-static analyses

These three structures have been conceived to have about a same, relatively low, seismic resistance, but are characterized by a decreasing capability of dissipating energy, progressing from case (A) to case (C). Therefore, the scope of structure (B) and (C), which may appear somewhat unusual according to local guidelines and codes of practice, is to provide a speculative comparison to the reference structure (A).

The fill is made of coarse-grained material with an angle of shearing resistance $\varphi' = 35°$, while the foundation soil is fine-grained with an angle of shearing resistance $\varphi' = 28°$ and an effective

cohesion c' = 10 kPa. The resistance at the soil-reinforcement contact is purely frictional with a friction angle φ'_S equal to that of the parent soil. A study of the effect of the strength at the soil-reinforcement interface was also carried out, using an interface strength factor of 0.7; it was found that this reduction in the contact strength has a negligible influence on the pattern of behaviour found in the reference analyses. All the materials are dry and have a unit weight $\gamma = 20$ kN/m^3.

To study the plastic mechanisms of each of the above mentioned schemes, finite different analyses were carried out in plane strain conditions using the computer code FLAC v.5 (Itasca, 2005). Pseudo-static analyses were performed increasing progressively the horizontal component of the inertial force until the strength of the system is fully mobilized and a plastic mechanism is activated. Figure 2 shows a detail of the calculation grid adopted for case (A): it has a total width of about 100 m and extends 40 m below the earth fill. In the static and pseudo-static analyses, both horizontal and vertical displacements were restrained at the base of the grid, while the horizontal displacements only were inhibited at the lateral boundaries. Soil behaviour was modelled as an elastic-perfectly plastic material with a Mohr-Coulomb plasticity criterion, assuming zero dilatancy, a Poisson ratio of 0.3 and a shear modulus equal to 20 ÷ 50 % of the small strain shear stiffness, depending on the computed average strain level.

The reinforcing levels were modelled using FLAC strip elements, which react only to axial tension. For these elements, the constitutive relationship between the axial force T and the axial strain ε in the strip is assumed to be elastic-perfectly plastic, with an equal yield strain ε_y for both walls of cases A and B. The contact at the soil-grid interface was simulated as elastic-perfectly plastic, with a very large stiffness K_s and a purely frictional strength with $\varphi'_S = \varphi' = 35°$.

Table 1 reports the mechanical properties of the reinforcements which are typical of a medium-strength PET geo-grid. The wall façade was assumed to behave as an elastic material and it was modelled by assigning a purely elastic behaviour to the couple of soil zones closest to the lateral surface of the reinforced structure.

The construction of the reinforced soil structure and of the fill was simulated in 25 steps, after initialising the effective stresses in the foundation soil; each step included the activation of a reinforcement element, the corresponding portion of wall facing, and a 0.6 m-thick soil layer; soil stiffness was then updated to account for the change in effective stresses after each construction step. The maximum horizontal displacement computed at the end of the construction phase was equal to 1.1% and to 1.0% of the wall height for case A and B respectively, while a value of 0.5% H was obtained for the non-dissipative wall (case C). Subsequently, an evaluation of safety with respect to a static collapse was carried out iteratively by reducing progressively the strength parameters of the soil (e.g. Callisto, 2010) and the soil-reinforcement contact; these analyses yielded similar values of the strength factor for the three structures, which was slightly lower than 1.25.

After the end of wall construction, a pseudo-static analysis was carried out applying a uniform horizontal body force expressed as a fraction k_h of gravity. The value of the seismic coefficient k_h was increased progressively until convergence, evidenced by a steady reduction of the unbalanced forces, became no longer possible. Under this circumstance, the numerical model

exhibited a well-defined mechanism, associated with a plastic flow of the soil. The seismic coefficient k_h that activates the mechanism is termed "critical" and is indicated as k_c. It must be noted that, due to the activation of a plastic flow in the critical conditions, the values of the computed displacements in the pseudo-static analyses have only a conventional meaning, as they refer to a system that is accelerating indefinitely.

Table 1. Mechanical parameters adopted for the geo-synthetic reinforcements.

	case (A)	**case (B)**
T_T (kN/m)	25	35
EA (kN/m)	1250	1750
ε_Y	0.02	0.02
φ'_S (°)	35	35
K_S (kN/m^2)	10^6	10^6

Table 2. Mechanical properties of the soil.

soil	**c′ (kPa)**	**φ′ (°)**	**B (kPa)**	**C (-)**	**D (-)**
foundation	10	28	12750	1397.4	0.790
fill	1	35	5100	5329.5	0.500

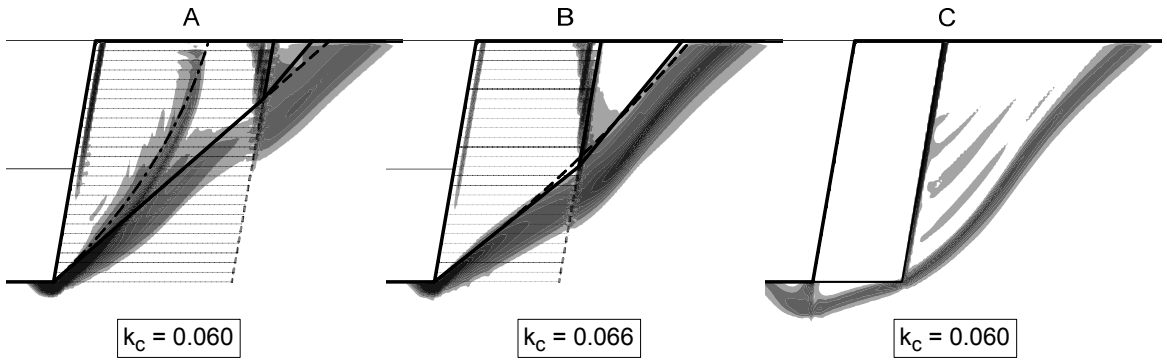

F

relevant in critical conditions)

Figure 3 shows the contours of shear strains γ obtained in critical conditions for the three structures of Figure 1, together with the corresponding values of critical seismic coefficient k_c. Although, the computed values of k_c are quite similar, ranging from 0.060 to 0.066, the deformation patterns appear to be very different; for case (A), two concurrent plastic mechanisms develop: the prevailing one intersects the reinforcements and closes up past them, with large strain gradients occurring at the contact between the backfill and the reinforced zone; the second one is entirely confined within the reinforced area and seems to be not fully developed, as smaller values of the strain contours can be observed near the top of the structure.

The two mechanisms converge towards the toe of the structure, with the foundation soil being only marginally involved. For case (B), only one, more evident plastic mechanism is observed, that develops from the lower portion of the reinforced structure, and mobilise the shear strength in most of the backfill. In case (C), since any internal failure is prevented, the mechanism can

involve only shear strength mobilisation of the foundation soil and of the backfill. Therefore, for the reference case (A), the results suggest that there are two concurring mechanisms. The prevailing one mobilizes the resistance of about 75% of the reinforcements and can be interpreted by a two-block scheme extending to the upper portion of the backfill. The secondary one is fully internal and is consistent with a log-spiral sliding surface mobilising the resistance of all the reinforcing levels. Since the two mechanisms are associated to similar strains levels, it can be reasonably assumed that both are capable to produce a significant amount of energy dissipation during an earthquake. On the other hand, case (B) shows only a single plastic mechanism, which attains the resistance of about half the reinforcing layers and extends considerably beyond the reinforced area, in accordance with a two-block scheme. Hence, the absence of concurring plastic mechanisms suggests that a smaller amount of energy dissipation can be expected. In case (C), any plastic mechanism can be developed only by mobilising the strength of the external soil, including the backfill and the foundation. Therefore, this idealised structures provides no internal energy dissipation and it is deemed to show the worst performance under seismic loadings.

Dynamic Behaviour

In order to asses whether the plastic mechanisms observed in the pseudo-static analyses are also representative of the deformation pattern when the structures are subjected to severe seismic loading, time domain dynamic analyses were performed using the same finite difference grid of the pseudo-static analyses. Starting from the end-of-construction stage, the horizontal fixities at the lateral sides of the grid were replaced by FLAC free-field boundary conditions in order to prevent waves reflection inside the domain. Dynamic calculation was carried out by applying time-histories $a(t)$ of the horizontal acceleration to the bottom boundary of the grid, using a time step $dt = 10^{-6}$ s. The scaled seismic record of Assisi (peak acceleration $a_{max} = 0.28$g, Arias Intensity $I_A = 0.75$ m/s, significant duration of Arias intensity $T_s = 4.28$ s) was employed as seismic input. Key feature of the selected record is that it has proved to be intense enough to activate the plastic mechanisms found in the previous pseudo-static analyses.

The cyclic behaviour of the soil was described through the hysteretic damping model implemented in FLAC, coupled with the same Mohr-Coulomb plasticity criterion used in the pseudo-static analyses. The hysteretic damping model is essentially an extension to two-dimensions of the non-linear soil models that describe the unloading-reloading stress-strain cycles using the Masing (1926) rules. The model requires the values of the small-strain shear stiffness and a backbone curve. The backbone curve was calibrated to reproduce the modulus decay curve published by Seed & Idriss (1970) for coarse-grained materials. The small-strain shear stiffness was expressed as a function of the mean effective stress p':

$$G_0 = B + C \times (p')^D \tag{1}$$

Values for the coefficients B, C, and D were selected to reproduce the typical small-strain stiffness for a medium plasticity sandy-silt for the foundation soil and a dense sand for the backfill. Table 2 lists the values of strength and stiffness parameters adopted in the analyses.
In the soil model, damping results from the hysteretic unloading-reloading cycle and is proportional to the maximum strain attained. Energy dissipation also occurs when the strength is

fully mobilized into the soil and at the soil-reinforcement interface. Finally, a small amount of additional viscous damping was used to attenuate the soil response at very small strains and to reduce spurious high-frequency noise. This was obtained by specifying a Rayleigh damping with both mass and stiffness components corresponding to a damping ratio of 1 % at a central frequency of 1.02 Hz, which is the fundamental frequency of the soil deposit, including the backfill.

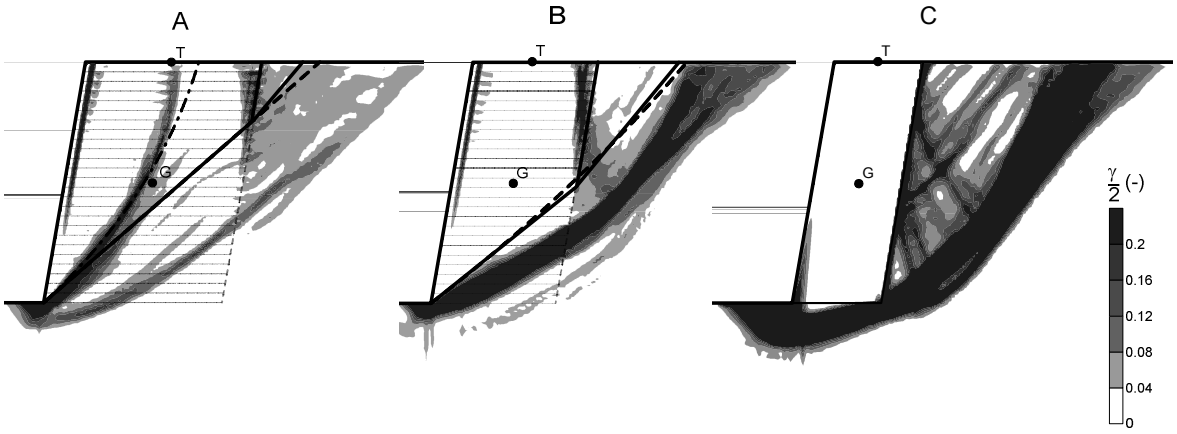

Figure 4. Dynamic analyses: contours of shear strains at the end of the seismic event

Figure 4 shows the contours of the shear strains computed at the end of the seismic record for the three schemes of Figure 1. The deformation pattern of case (A) is similar to the plastic mechanisms obtained from the pseudo-static analyses, with the development of two intensely sheared surfaces: the internal one is very close to the critical internal log-spiral emerged from the pseudo-static analysis, while the second surface is somewhat lower than the corresponding pseudo-static one, and engages a larger portion of the foundation soil. The shear strain contours of structure (B) show a two-block-mechanism which is analogous to that obtained for the pseudo-static critical condition, suggesting that the seismic behaviour is controlled by the activation of the same single plastic mechanism obtained from the pseudo-static analysis. Finally, the dynamic analysis of the non-dissipative structure (C) shows the activation of a plastic mechanism which is totally external to the wall and, again, very similar to the corresponding pseudo-static mechanism of Figure 3. Then it can be inferred that the plastic mechanisms activated in the three different structures by a uniform acceleration field are sufficiently indicative of the actual seismic response, provided that the reinforcing elements have a plastic ductility sufficient to accommodate the deformation of the structure. Masini *et al.* (2015) showed that the dynamic behaviour of case (A) changes dramatically if the analysis accounts for a loss of tensile strength of the reinforcement after an ultimate strain ε_u is reached. In this case, the reinforcements reach progressively their ultimate strain and an internal failure develops, leading the structure to collapse.

A comparison of the three different mechanisms depicted in Figure 4 indicates that, although the critical seismic coefficient for the three structures is about the same, the importance of internal plastic deformations decreases from case (A) to case (C); therefore, a general decay of the seismic performance should be expected as smaller amounts of kinetic energy can be dissipated

permanent horizontal displacements computed at the end of seismic loading for the centre of gravity G of the three structures (Figure 5). Structure (A) exhibits a permanent displacement u = 0.43 m, which is equal to 2.9% of the wall height H. Structure (B) and (C) undergo significantly larger displacements than those computed for case (A): 2.6 times for case (B), and up to 4.5 times larger for the non-dissipative structure (C).

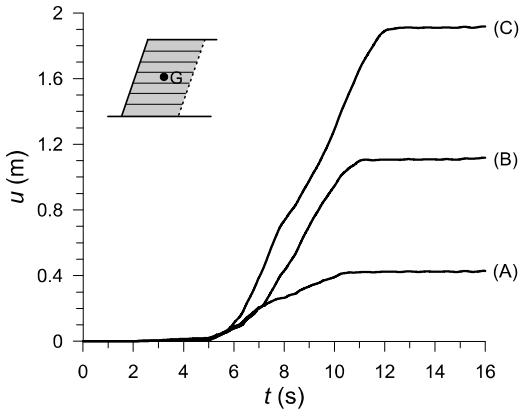

Figure 5. Time histories of permanent horizontal displacements

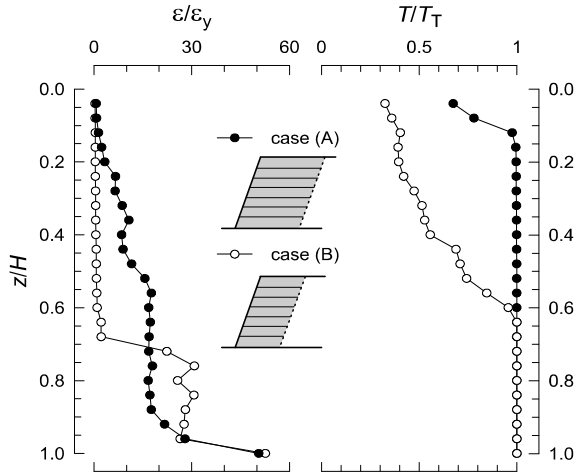

Figure 6. Profiles of mobilised strength T/T_T and of the corresponding strain ratio $\varepsilon/\varepsilon_y$

The presence of an internal plastic mechanism also affects the stress and strain distribution among the reinforcements. For the GRWs of case (A) and (B), Figure 6 shows the profiles of the mobilised tensile strength T/T_T of the reinforcements and of the corresponding maximum axial tensile strain ε, divided by the yield strain ε_y. Both T/T_T and $\varepsilon/\varepsilon_y$ refer to the post-seismic condition. For case (A), the strength of 90 % of the reinforcements is reached ($\varepsilon/\varepsilon_y > 1$, $T/T_T = 1$) due to the activation of the internal mechanism; the post-seismic axial strain increases with depth: in the lower half of the structure it is in the range of 15 to 20 times the yield strain ε_y, but in the lowest two levels it is as large as 30 to 50 ε_y. Conversely, for case (B) less than 50 % of the reinforcements reach their strength after the earthquake even though they undergo tensile strains significantly larger than for wall (A).

Therefore, the diffusion of plastic strains within the reinforced soil improves significantly the overall dissipative capacity of the system. However, the development of internal plastic mechanism and, more generally, the good seismic performance of the structure is strictly dependent on the ductility of the reinforcements, which should be designed to sustain large deformations without undergo sensible strength reduction. This principle can be regarded as an extension to GRWs of the performance based design which is already well established for other structure of civil engineering.

Conclusion

Geosynthetic-reinforced retaining walls subjected to intense seismic loadings develop permanent displacements which can be considered as the result of subsequent transient activations of plastic mechanisms. Pseudo-static methods can be profitably employed to predict such plastic mechanisms, provided that they are used iteratively (Callisto, 2014). In this context, limit analysis and limit equilibrium solutions can be advantageously extended to pseudo-static conditions and used to analyze the activation of concurrent mechanisms (Masini et al., 2015).

Pseudo-static analyses carried out using the critical seismic coefficient that activates the plastic mechanisms represent an effective tool to understand the actual deformation pattern resulting from the time-domain dynamic analyses. Using this approach, it was shown that the three different structures examined in this paper are characterized by about the same critical seismic coefficient, but exhibit very different seismic behaviours. Specifically, the reference structure (A) undergoes a composite deformation pattern that includes two concurrent plastic mechanisms, a prevailing one that can be interpreted by a two-block scheme partially developing behind the reinforced zone, and a secondary one which is fully internal; conversely, it was found that the seismic behaviour of both structures (B) and (C) is controlled by a single, well defined mechanism, which is partly internal for structure (B) and totally external for structure (C).

Different pseudo-static plastic mechanisms of the three structures result in different behaviours under dynamic loading. Specifically, the reference wall (A) shows the best seismic performance with maximum horizontal displacements of 0.03 H. Conversely, wall (B), which has shorter but stronger reinforcements, undergoes larger displacements (0.075 H) as the development of the internal plastic mechanism is partly inhibited and an important source of energy dissipation is lost. Then, structure layouts entailing more than one mechanism should be preferred for an effective seismic design and this can be fulfilled by preferring long reinforcements with a relatively low strength. Finally, structure (C) can mobilize only external mechanisms, without any internal energy dissipation, even if it has the same overall seismic strength of structure (A). As a result, it exhibits the worst seismic performance, with permanent displacements sensibly larger than those shown by the GRWs (0.13 H). This finding is consistent with field observations, indicating a generally better performance of reinforced earth structures if compared to the behaviour of more conventional reinforced-concrete retaining walls. However, the results of the dynamic analyses showed that during severe seismic actions the reinforcements can experience large elongations and thus the seismic behaviour of GRWs is critically dependent on the ductility capacity of the reinforcing levels. Therefore, the choice of the most appropriate reinforcement should be made principally on the basis of the maximum elongation that it can sustained without appreciable strength reduction.

Acknowledgments

This research work presented in this paper was partly funded by the Italian Department of Civil Protection under the ReLUIS 2009-2012 research project.

References

Callisto L. A factored strength approach for the limit states design of geotechnical structures. Canadian Geotechnical Journal 2010; 47(9):1011–1023.

Callisto L. Capacity design of embedded retaining structures. Géotechnique 2014; 64:204–214.

Itasca. *FLAC Fast Lagrangian Analysis of Continua v. 5.0.* User's Manual, 2005.

Koseki J, Nakajima S, Tateyama M, Watanabe K, Shinoda M. Seismic performance of geosynthetic reinforced soil retaining walls and their performance-based design in Japan. Proc. Performance-Based Design in Earthquake Geotechnical Engineering, Tokyo, 149-161. London: Taylor & Francis Group, 2009.

Ling HI, Mohri Y, Leshchinsky D, Burke C, Matsushima K, Liu H. Large-scale shaking table tests on modular – block reinforced soil retaining walls. Journal of Geotechnical and Geoenvironmental Engineering, 2005. ***131****(4):465-476.*

Masini L, Callisto L, Rampello S. An interpretation of the seismic design of reinforced-earth retaining structures. Geotechnical Earthquake Engineering, Géotechnique symposium in print, 2015. Géotechnique 2015; 65(5):349–358; doi:http://dx.doi.org/ 10.1680/geot./SIP 15-P-001.

Masing G. Eigenspannungen und Verfertigung bim Messing. Proceedings 2nd Int. Congress on Applied Mechanics, 1926. 322-355. Zurich-Leipzig: Füssli (in German).

Seed HB, Idriss IM. *Soil moduli and damping factors for dynamic analysis.* Report No. EERC 70-10, Berkeley, CA, USA: University of California, 1979.